Author/s:
Zhang, H;Cadusch, J;Kinnear, C;James, T;Roberts, A;Mulvaney, P

Title:
Direct assembly of large area nanoparticle arrays

Date:
2018-08-28

Citation:
Zhang, H., Cadusch, J., Kinnear, C., James, T., Roberts, A. & Mulvaney, P. (2018). Direct assembly of large area nanoparticle arrays. ACS Nano, 12 (8), pp.7529-7537. https://doi.org/10.1021/acsnano.8b02932.

Persistent Link:
https://hdl.handle.net/11343/299419

Direct Assembly of Large Area Nanoparticle Arrays

Heyou Zhang[1], Jasper Cadusch[2], Calum Kinnear[1], Timothy James[2,3], Ann Roberts[2], Paul Mulvaney[1]*

[1] ARC Centre of Excellence in Exciton Science, School of Chemistry, University of Melbourne, Parkville, Vic. 3010, Australia.

[2] School of Physics, University of Melbourne, Parkville, Victoria 3010, Australia.

[3] Reserve Bank of Australia, Craigieburn, Victoria 3064, Australia.

*e-mail: mulvaney@unimelb.edu.au

ABSTRACT:

A major goal of nanotechnology is the assembly of nanoscale building blocks into functional optical, electrical or chemical devices. Many of these applications depend on an ability to optically or electrically address single nanoparticles. However, positioning large numbers of single nanocrystals with nanometre precision on a substrate for integration into solid-state devices remains a fundamental roadblock. Here, we report fast, scalable assembly of thousands of single nanoparticles using electrophoretic deposition. We demonstrate that gold nanospheres down to 30 nm in size and gold nanorods < 100 nm in length can be assembled into pre-defined patterns on transparent conductive substrates within a few seconds. We find that rod orientation can be preserved during deposition. As proof of high fidelity scale-up, we have created centimetre scale patterns comprising more than 1 million gold nanorods.

KEYWORDS:

nanoparticles, arrays, electrophoretic deposition, plasmonic, polarization, scale-up.

Nanoscale particles exhibit unusual, size-dependent optical, luminescent, magnetic, catalytic or electronic properties. As a result, there is considerable scope for the application of these materials in fields such as nanoelectronics,[1] biosensors,[2-4] ultrasensitive biodiagnostics,[5] chiral sensors,[6] high-density information storage,[7] plasmonic solar cells,[8] and full-colour plasmonic pixels for displays.[9,10] However, while much attention has focussed on the synthesis and characterisation of a wide range of nanocrystals over the last two decades, there has been less emphasis on the equally important challenge of nanocrystal assembly. The key challenge is to precisely control assembly of individual molecular building blocks at the nanometre lengthscale.[11] These building blocks may be quantum dots, metal nanocrystals, biomolecules, single virus particles, polymers, DNA strands or hybrid inorganic-organic structures. The spacing between these nanoscale building elements is often quite critical. For example, by specifically controlling the distance between particles, plasmonic pixels made from aluminium nanorods are capable of producing a range of monochromatic colour responses.[9,10]

Thermal evaporation is one of the most commonly used techniques for creating arrays of nanostructures on lithography patterned template.[12] This method provides a "top-down" pathway for fabrication. However, thermal evaporation is restricted by the cost, the roughness of the deposited films and the limited choice of suitable target materials.[13] In principle, directed, "bottom-up" assembly provides much greater flexibility.[14] Directed assembly is a method to assemble existing nanoscale materials onto a pre-patterned substrate by application of external forces. The goal is to maintain the original morphology of the materials during the fabrication and to use the external forces to push the materials into pre-patterned templates. It is possible to apply this approach to differently shaped materials such as spheres, rods, stars and other complex particles such as alloys and core-shell materials. Moreover, by choosing suitable forces, directed assembly can be applied to a wide range of materials.[15-17] There are several promising sources of such external fields including capillary forces,[18] chemical forces[19], electrophoretic forces[20] and optical tweezing. [21]

To date such assembly has only been demonstrated on small scales. For example, Kuemin *et al*.[22] and Flauraud *et al*.[23] successfully assembled gold nanorods (NRs) using capillary force assembly (CFA). By controlling the process parameters, particles were assembled and oriented into pre-patterned substrates. However, CFA is extremely sensitive to surface roughness and to surface contaminants, which cause both contact line pinning and mis-assembly.[18] Another approach is chemically directed assembly (CDA). CDA exploits the

attractive chemical interactions between particles and the substrate to effect assembly as demonstrated by Nepal *et al*.[19] Their approach relies on the particles sampling the pre-fabricated wells at some point along their diffusive trajectories and becoming adsorbed to the adhesive coating. In theory, this method is ideal for all kinds of material fabrication, as long as the particles and substrate have been functionalized properly. However, the deposition rates are often slow and non-specific adsorption leads to high levels of background noise. Creating chemistry that is specific for each type of particle-substrate combination is also challenging.

The third directed assembly approach is electrophoretic deposition (EPD). EPD has many advantages. For example, it offers rapid processing and there is little restriction on the particle type or substrate. Furthermore, it uses simple apparatus and is easy to apply.[24] A standard EPD process for 15 nm thin film fabrication requires only a few minutes. The thickness of the film can be precisely controlled by tuning the parameters of the EPD process such as applied voltage, particle concentration, and deposition time.[25] Furthermore, EPD has been reported as a versatile process for many kinds of materials, including ceramic powders,[26] metallic particles,[27] polymers[28] and semiconductor materials.[29] Solomon and co-workers have studied the assembly of colloidal microcrystals[30] and liquid crystals[31] under direct current electric field, while Prieve and co-workers have developed the fundamental theory for nanoparticle EPD assembly.[32,33] It thus appears that EPD could be a promising approach for nanomaterial fabrication. However, to date, most effort has focussed on deposition of larger micron scale particles. In 2009, Barbee *et al*.[28] reported a method to deposit 0.5 μm polystyrene (PS) micro-beads into an Au coated silicon wafer with a patterned photoresist blocking layer on top. They successfully used EPD to directly deposit these micro-beads into an array. Later on, the kinetics of this deposition process were also studied by Qian *et al*.[34] They found that the voltage and particle-to-hole size ratio determined the quality of the PS bead deposition. Finally, Xiong *et al*.[35] demonstrated that lines of silica nanoparticles could be deposited into an EBL template. However, they did not achieve single nanoparticle resolution, nor could they demonstrate orientational control. Those reports provided proof-of-concept that the combination of EPD and a patterned template is a useful technique for single particle assembly. However, extension to nanoscale assembly is highly challenging. Brownian motion can severely hamper particle deposition while double layer effects dominate the nanoparticle-surface interactions. Furthermore, it is impossible in

general, to watch single nanoparticles during deposition, which renders optimization of the assembly process extremely difficult.

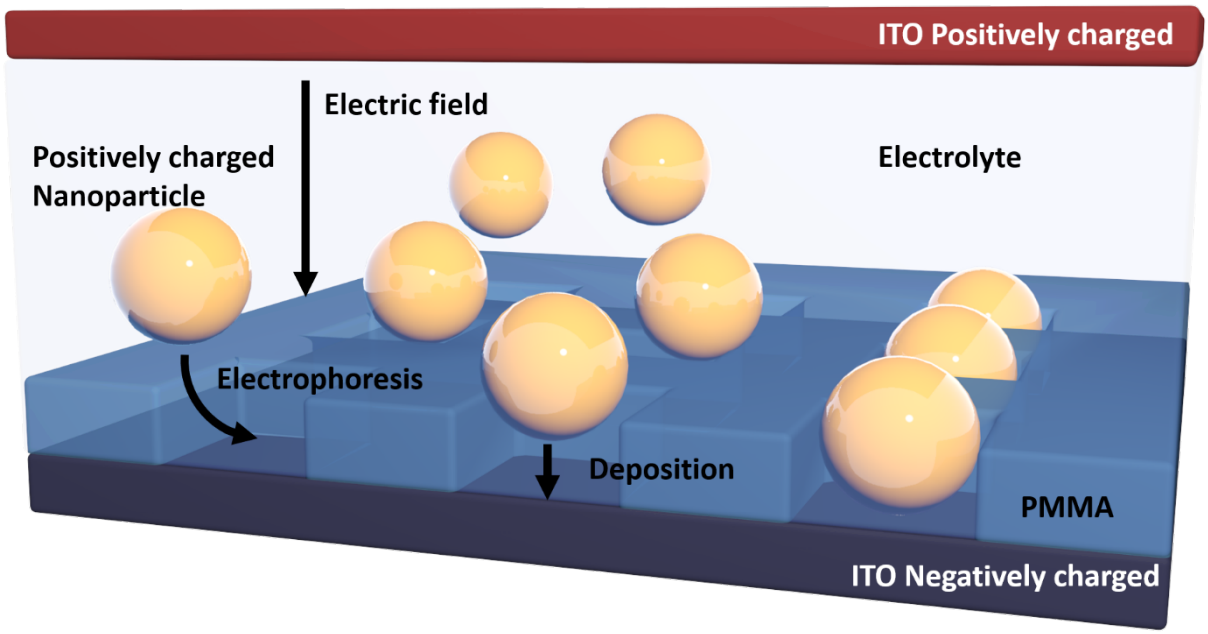

Figure 1. Schematic of the EPD process showing nanospheres deposited onto EBL fabricated ITO-PMMA template (dimensions not to scale). A controlled volume of nanoparticle colloidal solution mixed with controlled concentration of NaCl electrolyte is confined between an EBL patterned ITO-PMMA template and an ITO counter electrode on the top. Nanoparticles are positively charged by coating poly-dimethyl-diallyl ammonium chloride (poly-DADMAC). An electric field is generated by applying a potential between the ITO-PMMA template and the ITO counter electrode.

In this article, we demonstrate a highly efficient method for large area assembly of *single* gold nanoparticles (spheres and rods) into a pre-patterned poly-methyl methacrylate (PMMA)-indium tin oxide (ITO) template *via* EPD. We also demonstrate real-time monitoring of nanocrystal EPD under dark-field microscope (Supp Info movie file).

The EPD cell comprised an ITO electrode and a second electron beam lithography (EBL) patterned PMMA-ITO electrode, with positively charged gold nanoparticles dispersed in an aqueous electrolyte between the electrodes (Figure 1). A DC potential difference was applied between the electrodes to generate an electric field. Under the influence of this electric field, particles underwent electrophoresis and were deposited into the nanoscale cavities patterned onto the template.

RESULTS AND DISCUSSIONS

The primary assembly of the gold nanoparticles *via* EPD employed 40 × 40 square arrays of 120 × 120 nm box cavities (Figure S2a). Figure 2a shows a dark field microscope image of the array filled with 110 nm gold nanospheres (NS) after deposition. Since near-field optical coupling of nanoparticles is dependent on the size of the gap between each particle and the centre-to-centre distance between each cavity is 4 μm, we can clearly observe the optical response of each individual particle inside the array. The array was filled with gold NSs with uniform yellowish scattering light, and non-specific binding was minimal. A scanning electron microscope image of part of the gold nanosphere array consisting of nine wells is shown in figure 2b. Each cavity was filled with only one particle, and all nine gold NSs were located inside cavities. The single particle scattering spectrum was also measured for the deposited gold NSs. Figure S5a presents normalized scattering spectra for ten gold NSs. We randomly chose ten particles to verify the quality and consistency of EPD assembled gold NSs. The scattering spectra all evince a similar peak around 600 nm, which is correlated to the reported scattering spectrum of a single 110nm gold NS.[36] We found that EPD is self-terminating. Deposition of a nanoparticle into a surface well apparently blocks the electric field and consequently only single particles are deposited.

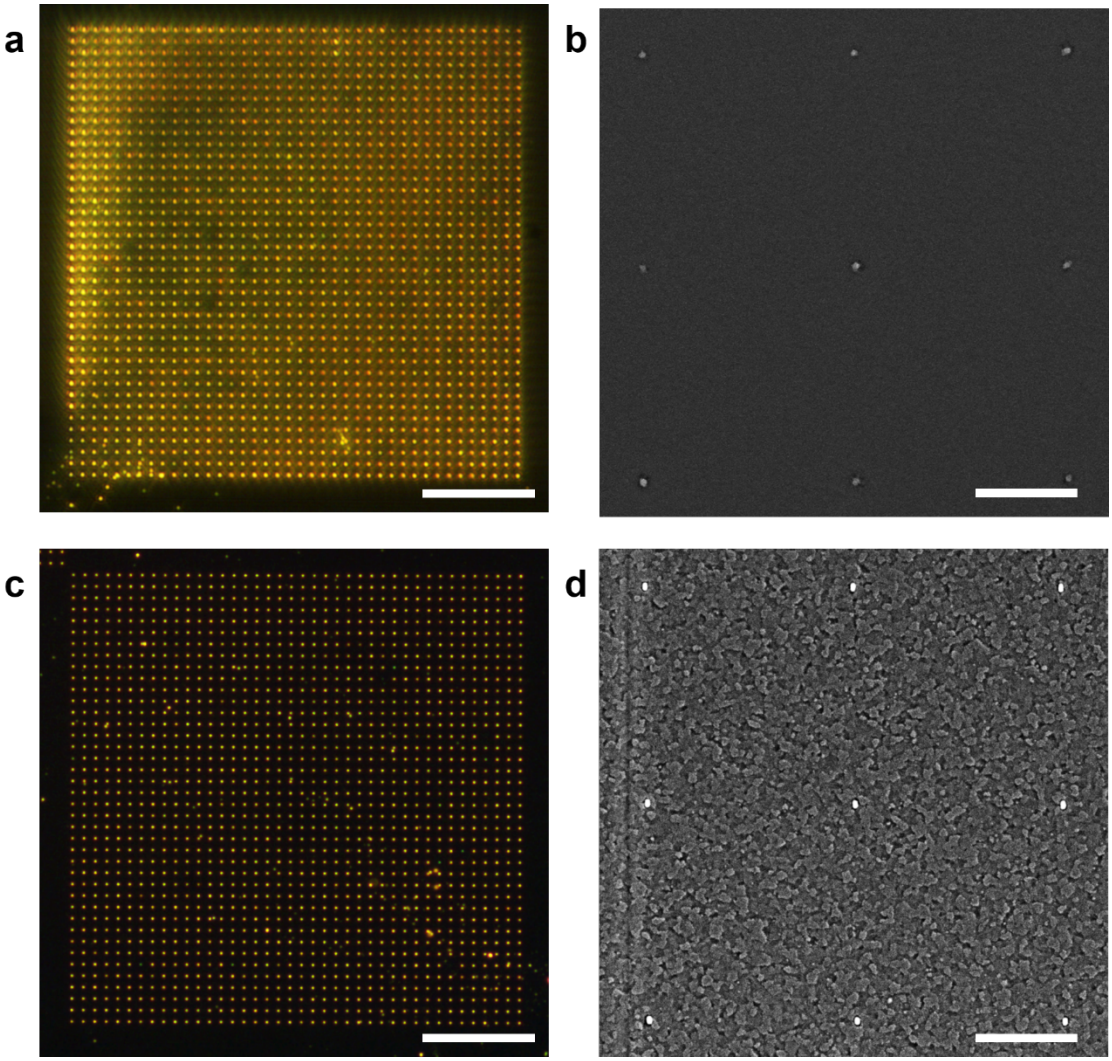

Figure 2. Results of gold NSs and gold NRs arrays fabricated *via* EPD direct assembly (a) Dark-field image of a 40 × 40 box array filled with 110 nm gold NSs. (b) SEM image of several gold NSs in the array from Figure 1a. (c) Dark-field image of a 40 × 40 gold NRs array filled by 100 nm × 40 nm gold NRs. (d). Scanning electron microscope image of several gold NRs in the array of Figure 1c. (Scale bar: Dark-field imges, 40 μm; Scanning electron microscope imgaes, 2 μm)

Compared to gold NSs, gold nanorods are more appealing because of their anisotropic optical properties. We also assembled arrays of gold NRs *via* EPD and Figure 2c shows a dark-field image of an array filled with 100 × 40 nm gold NRs. The design of the template is similar to the templates used for gold NSs deposition but with rectangular rather than square cavities (Figure S2b). Typically, the dimensions of the cavities are about 10% larger than the particle dimensions. The separation between each rod in the array is 4 μm, enabling individual rods to be easily distinguished by dark-field microscopy. The primary colour seen in reflection is due to the strong surface plasmon resonance at 720 nm for 100 × 40 nm gold NRs. Only a small number of background particles sticking at the PMMA surface could be observed.

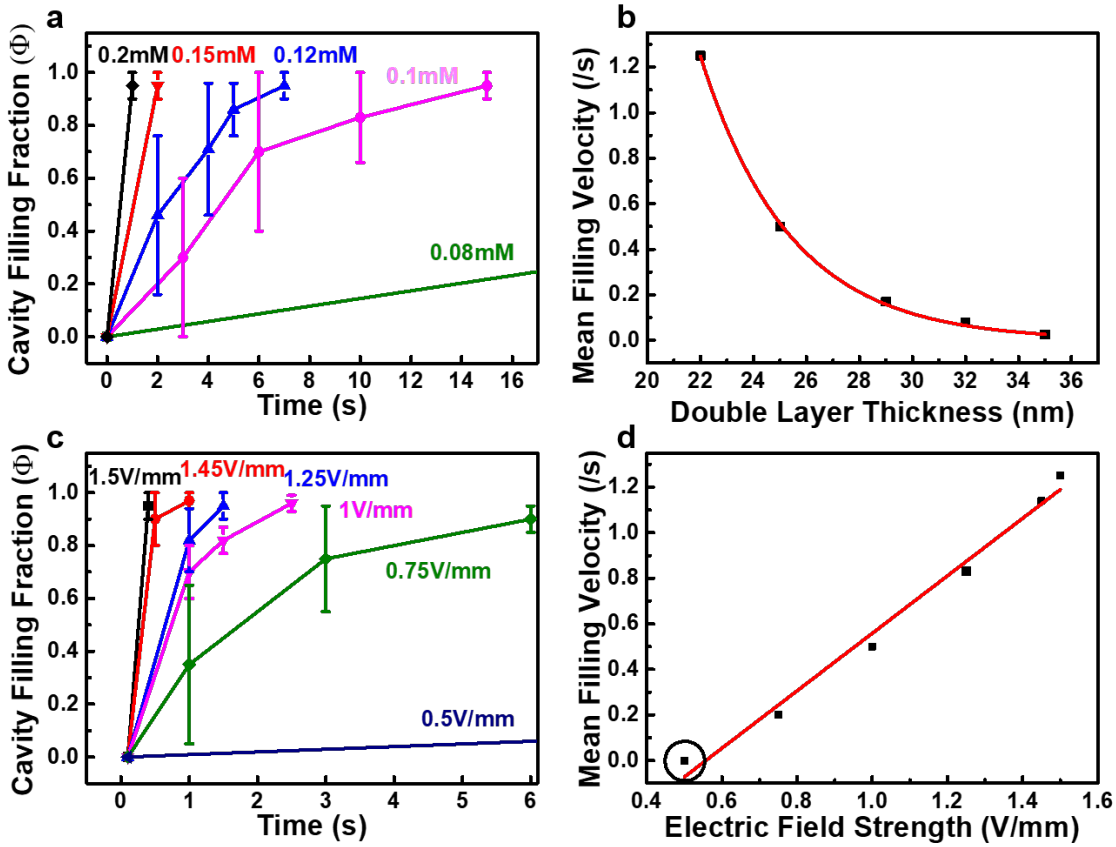

Figure 3. Parameter studies of the EPD process (a) Plot of the cavity filling fraction φ as a function of time for different NaCl concentrations (Electrode spacing = 2 mm, mean gold nanosphere diameter = 110 nm, gold nanosphere concentration = 30 µg/mL, applied potential = 3 V, T = 293 K, pH = 7, aqueous phase). (b) Plot of the mean filling velocity as a function of the electrical double layer thickness. (c) Plot of the cavity filling fraction φ as a function of time for different electric field strengths (Electrode spacing = 2 mm, NaCl concentration = 0.2 mM, gold nanosphere concentration = 30 µg/mL, T = 293 K, pH = 7, aqueous phase). (d) Plot of the mean filling velocity as a function of the applied electric field. (All error bars indicate 5 standard deviations around the mean value for each data point).

Figure 2d shows a scanning electron microscopy image of a region of the gold nanorod array. The image highlights the fact that gold NRs can be precisely positioned and aligned within each cavity, and furthermore each cavity is again filled by only one gold NR. The gold NRs were aligned in the same orientation as the cavities. Ten gold NRs from one row of the array were randomly chosen and their individual scattering spectra recorded (Figure S5b). The overlapping of all ten spectra again demonstrates both the successful assembly of gold NRs and their high degree of monodispersity.

In order to understand and control the EPD assembly process, key parameters in the gold nanoparticle EPD process were also investigated to optimize and predict the assembly. According to the Smoluchowski equation [37,38] (eq.1), the mobility of a charged particle, μ, is defined as the ratio of the speed of the particle, v, to the magnitude of the applied electric field, E, and is given by:

$$\mu = \frac{v}{E} = \frac{2}{3}\frac{\varepsilon_0 \varepsilon_r \xi}{\eta} f(\kappa r) , \qquad (1)$$

where ε_0 is the vacuum permittivity, ε_r is relative permittivity of the solvent, η is the viscosity of the solvent and $f(\kappa r)$ is a function, which depends on the particle radius (r) and the electrical double layer thickness (κ^{-1}).[38] For aqueous electrophoresis, the mobility of a particle is influenced by (a) the applied electric field strength E, (b) the particle's zeta potential ξ and (c) the double layer thickness of the particle. Figure S6 shows the changes in the measured zeta potential and double layer thickness as a function of NaCl concentration. The double layer thickness is given by equation (2): [39,40]

$$\kappa^{-1} = \left(\frac{\varepsilon \varepsilon_0 kT}{2cz_i^2 e_0^2}\right)^{\frac{1}{2}} \qquad (2)$$

where k is the Boltzmann constant, T is the temperature, z_i is the ion charge, e_0 is the elementary electron charge and c is the concentration of 1-1 electrolyte. When the concentration of NaCl is increased, the thickness of the diffuse electrical double layer is decreased. To investigate the effects of electrolyte concentration and electric field strength on single nanoparticle EPD, we have measured the cavity filling fraction (defined as the ratio of filled cavities to the total number of cavities) under different experimental conditions (Figure 3). For each data point in Figures 3a and 3c, fresh PMMA-ITO templates were used. Note that each 4mm x 4mm template consists of 24 arrays and each array comprises 40 x 40 nanocavities. The assembly process was stopped after a certain time period. The filled cavities were counted in 10 arrays across the template by collecting dark field images and analysing them using Image-J software. This was repeated 5 times using 5 fresh templates for the same period of assembly. This is to reduce the errors associated with timing the deposition process. Hence each data point represents the observed fraction filled for 80,000 cavities. The error bars show the differences in filling fraction across the 5 templates. Due to the finite resistance of ITO, there is a potential gradient across the PMMA-ITO template and arrays closer to the connecting wires at the template edges typically exhibit higher filling fractions than those in the middle of the template.

Figure 3a shows the influence of electrolyte concentration on the filling rate at a fixed gold particle concentration (30 μg/mL) and fixed electric field (1.5 V/mm). When 0.2 mM or 0.15 mM NaCl was present, deposition occurred within 1 or 2 seconds (black and red lines in Figure 3a). However, when the NaCl concentration was reduced to 0.08 mM, the gold particles deposited much more slowly (blue, pink and green curves in Figure 3a). In Figure 3b, we plot the mean filling velocity as a function of the double layer thickness. Increasing the electrolyte concentration in the EPD system increased the filling rate, as expected. However, within the range of NaCl concentrations from 0.08 mM to 0.2 mM, the zeta potential of gold colloid remained close to + 44 mV ± 2 mV. Hence, from eq.1, the primary effect of increasing the electrolyte concentration during EPD is to increase $f(\kappa r)$, which in turn increases the gold nanoparticle mobility. However, there is an important second consequence. Higher electrolyte concentrations (thinner double layer thicknesses) facilitate access of the nanoparticles into the cavities because this process is accompanied by double layer compression, which is energetically unfavourable.

Another crucial factor, which influenced the EPD process, was the applied potential. The time to completely fill all cavities decreased when the applied potential was increased (Figure 3c), as expected from eq.1. A linear relationship between the mean filling velocity and the electric field strength was observed, as shown in Figure 3d. However, when the applied potential was decreased to 0.5 V / mm (circled point in Figure 3d), there was no deposition. This means there is a “turn on” potential for EPD assembly. This “turn on” potential is necessary to overcome the Brownian motion of the nanoparticles and the repulsion associated with entry into the nanocavity. This process will be examined in more detail elsewhere.

The electrolyte concentration and applied potential have extremely strong effects on the deposition process and quality of the filled arrays. During parameter optimization, we observed that lower NaCl concentrations and higher applied potentials led to greater non-specific particle deposition onto the PMMA surface, as shown in Figure S7. This is explained in terms of double layer screening. At low electrolyte concentrations and higher applied potentials, the electric fields generated in the cavities overlap in the surface region between the cavities and this can be strong enough to drive particles to adsorb onto the PMMA. Lower potentials and shorter Debye screening lengths ensure the gold rods are driven more efficiently into the cavities.

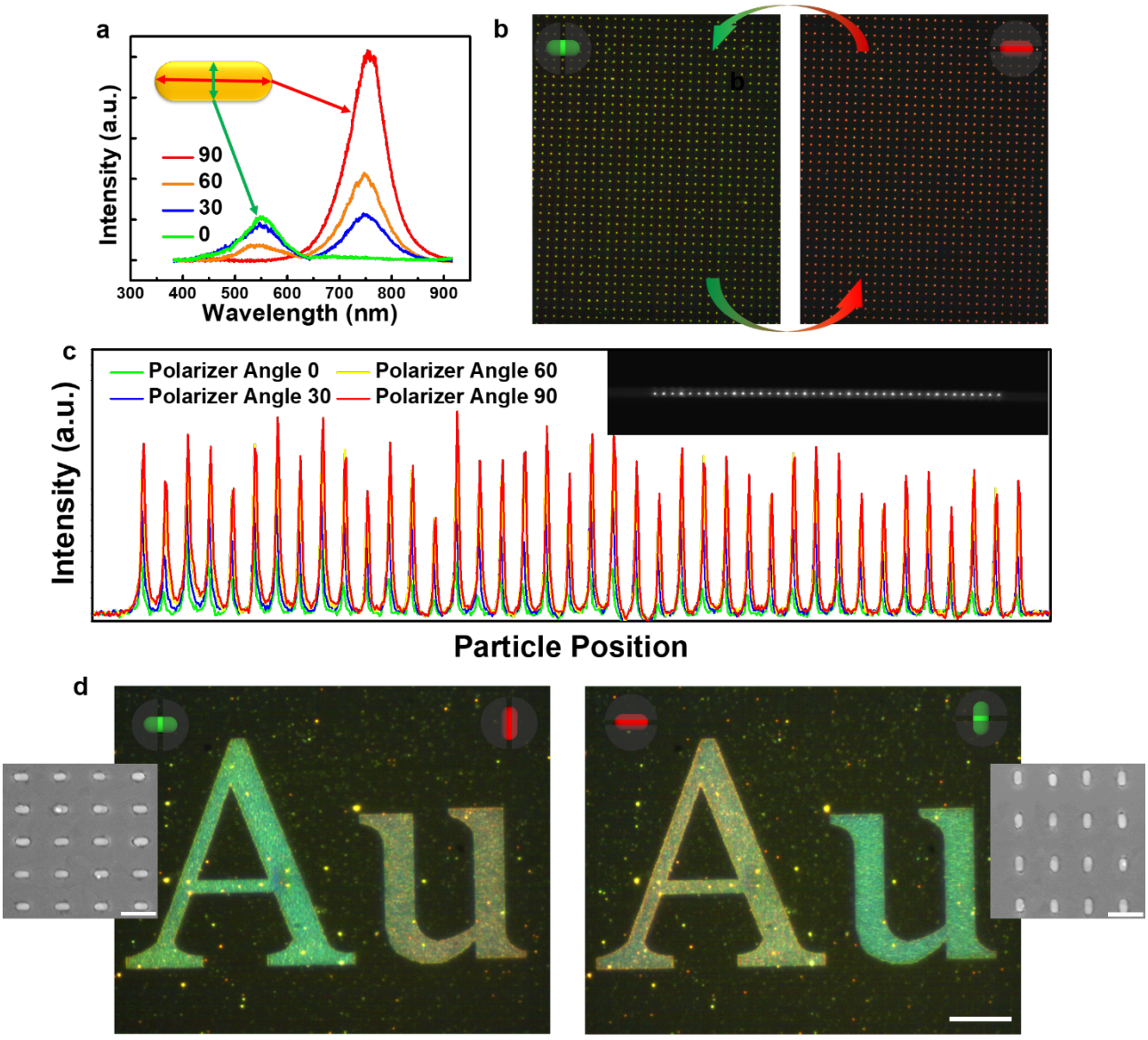

Figure 4. Polarization-dependent optical properties of gold NRs array. (a) Scattering spectra of a single gold NR at different polarization angles. (b) Dark-field images of a gold NR array under 0° (left) and 90° (right) polarization. (c) Broadband intensity changes in a line of gold NRs for different polarization angles. (d) Dark-field images at 0° (left) and 90° (right) polarization angles of the letters "A" and "u" assembled from gold NR arrays with perpendicular orientations (Scale bar: 10 μm). Inserts: corresponding scanning electron microscope images of parts of the arrays containing the letters "A" (left) and "u" (right) respectively (Scale bar 300 nm).

The quality of the gold NR assembly was further investigated by polarized dark-field microscopy. (A simplified schematic showing the set-up of the reflection-mode dark-field microscope is provided in Figure S8.) Figure 4a presents the intensity changes in the

scattering from single gold NRs for a series of polarization angles. At 0°, the polarizer is orthogonal to the major axis of the gold NRs and therefore, the intensity of the transverse scattering peak dominates, causing the gold NRs to appear green (scattering peak at 530 nm). Conversely, upon rotation of the polarizer to 90°, the perceived colour of the gold NRs is dominated by the longitudinal surface plasmon oscillations and the rods appear red (720 nm). Because the cavities were all oriented in one direction, all the particles deposited in the cavities should follow the same polarization-dependent colour changes. This is confirmed in Figure 4b. As we rotated the polarizer from 0° to 90°, the colour of the gold NRs is uniformly modulated from green (Figure 4b left) to red (Figure 4b right). This uniform colour change over the entire array indicates that the gold NRs were reproducibly deposited and aligned into cavities *via* EPD. We also used dark-field microscopy to investigate the broadband intensity changes of a row of gold NRs in an array as shown in figure 4c. When the polarizer was at 90°, all 40 particles displayed the highest intensity (red curves). Upon rotation of the polarizer by 30° to 60°, the scattering intensity decreased correspondingly (yellow curves). A further shift to 30° led to a further intensity decrease (Blue curves). Finally, when the polarizer was rotated to 0°, the spectra exhibited the lowest intensity (Green curves). This polarization-dependent intensity change occurs because the longitudinal mode is far more intense than the transverse mode of the gold NRs. To further confirm that the template determines the gold NR orientation, a pattern was created in the form of the letters “A”, and “u”, with the cavities being oriented perpendicular to each other in the two letters. In letter “A” the cavities are orientated horizontally and in the letter “u” they are orientated vertically. The letters were assembled using gold NRs with 300 nm edge to edge spacing between each rod as shown in figure S9.

Note that in Figure 4b, the spacing between the gold rods is several microns and each particle is fully resolved in the dark field microscope. The scattered colours correspond to the surface plasmon modes of the isolated gold nanorods. However, in Figure 4d, to create stronger contrast in the optical image, the particles are much closer together, with a separation between the ends of the gold rod ends being just 300 nm. Plasmon coupling pushes the longitudinal mode towards the NIR and the red colour is therefore weakened and the scattered colour that is observed tends to be more orange-red. There is also a slight red-shift in the transverse mode, which leads to a stronger perceived green colour. Hence the colours in Figures 4b and 4d are not the same due to different packing densities. However, the

uniform colour switching between the letters “A” and “u” upon rotation of the polarizer proves that the rods are uniformly oriented in the films.

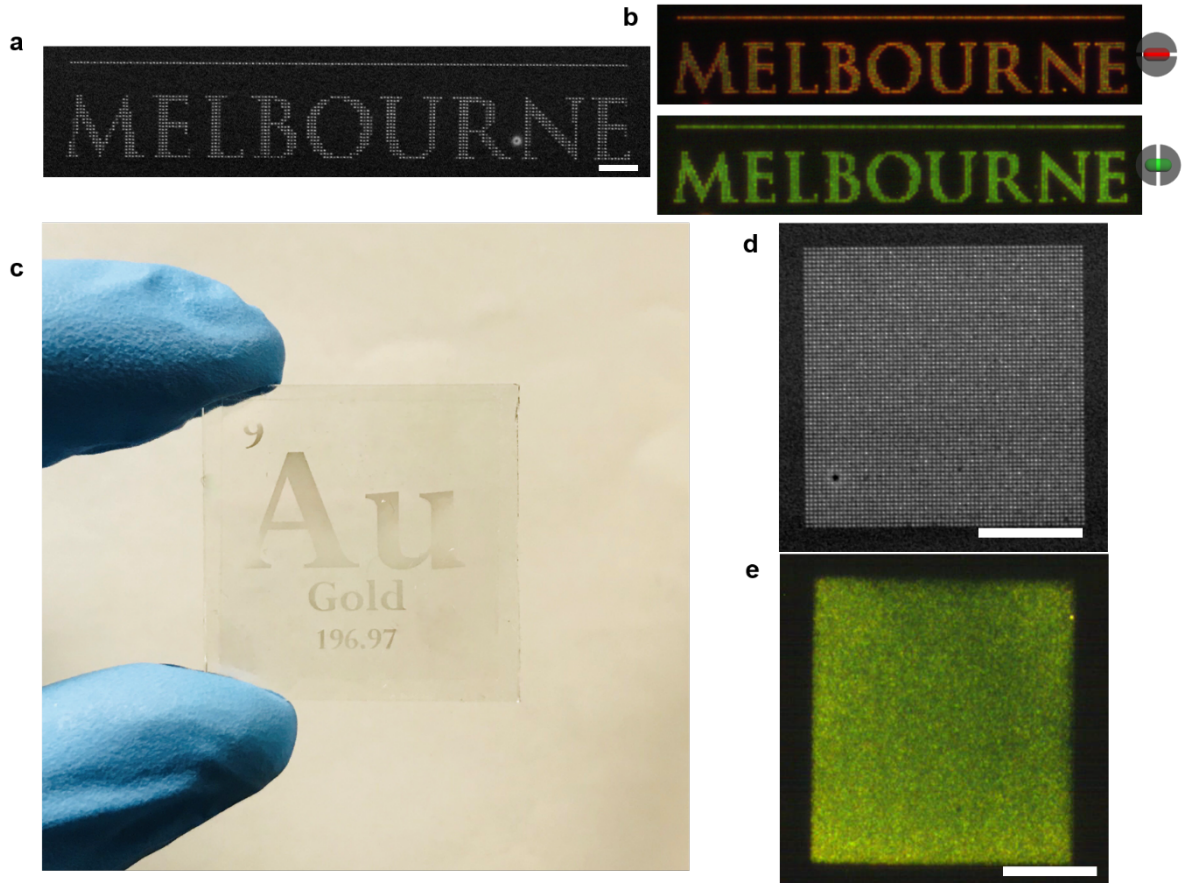

Figure 5: Large area Assembly (a) Scanning electron microscope image of the word “Melbourne” created from an array of single gold NRs. (b) Dark-field microscopy image of the text under vertical (top) and horizontal (bottom) polarization. (c) Digital picture of “Au” logo made by EPD on 25 mm × 25 mm ITO-PMMA glass slide. The left hand lines are 1 mm markings. (d) Scanning electron microscopy image of one 20 micron pixel of the “Au” logo showing a 66 × 66 array of single gold NRs. (e) Dark field microscopy image of one pixel of “Au” logo with 66 × 66 gold NRs filled. Scale bar: 10 µm.

To demonstrate the fidelity and potential for scale-up, we have constructed the text “Melbourne” from single nanorods, as shown in Figure 5a. The total scale of the logo is 100 µm in length and the image comprises 1125 cavities. Figure S10 presents a high magnification scanning electron microscope images of the logo filled by gold NRs. The single gold NRs were horizontally aligned. Again, a strong polarization dependence was observed under dark-field illumination (Figure 5b). The spacing between the gold rods in

Figures 5a and 5b is again 300 nm, which leads to weak surface plasmon coupling. The colour of the logo switches from orange-red (longitudinal mode) to stronger green (transverse mode) according to the angle of the polarizer. The ensemble scattering spectrum of the logo also exhibited strong scattering intensity changes depending on the polarizer angle (Figure S11).

Because the actual particle coverage in Figure 5a was much less than a monolayer and the entire logo was only 100 μm across, the colour could not be discerned by the naked eye. In order to fabricate a pattern which could be seen by the unaided eye, we designed and assembled an "Au" logo with dimensions 2.5 cm × 2.5 cm (Figure 5c). This "Au" logo is composed of arrays of pixels. Each pixel is an array containing 66 × 66 cavities with a smaller 200 nm end-to-end separation between cavities and filled with gold nanorods using EPD. Figures 5d, S12a and S12b present sets of scanning electron microscope images of the "Au" logo at different magnifications. More than 98% of the array cavities are filled with single gold nanorods. Figure 5d also shows a scanning electron microscope image of one pixel of the gold NR array. Because of the dense packing, the plasmon modes in the rods are strongly coupled and the letters are visible to the unaided eye and, in reflection, the image exhibits a dull gold colour despite being only a single monolayer thick. There are more than 1 million gold rods in this image, the first macroscopic image to be written in single nanoparticles. Figure 5e shows one pixel under the dark-field microscope. To see the scattered light from such monolayer of gold rods with the human eye requires closer packing of the gold rods. With 200 nm end-to-end separation, the pixels evince a greenish-yellow hue and the dark field spectrum exhibits a broad scattering peak at around 580 nm (Figure S12c).[41]

CONCLUSIONS

We have demonstrated that electrophoretic deposition can be used to assemble thousands, indeed millions, of single nanoparticles per second with nanometre spatial resolution into pre-patterned cavities or wells. The cavities can be used to control nanoparticle deposition by size, shape and orientation. The efficiency of the deposition process is very strongly dependent on the field strength and the electrolyte concentration. Scalability has also been demonstrated over 7 orders of magnitude with single nanoparticles being positioned with an accuracy of a few nanometres over centimetre areas.

METHODS

Gold Nanocrystal synthesis

Gold nanospheres (NS) with average 110 nm diameters were synthesized according to literature protocols.[36] Briefly, 20 mL ethylene glycol (Ajax Chemicals, 99.8%) was added into a glass flask and stirred with a magnetic bar. Then 0.8 mL of 1 M H_3PO_4 solution and 0.4 mL of poly-dimethyl-diallyl ammonium chloride (poly-DADMAC) (Sigma-Aldrich, 20 wt% in H_2O, Mw = 400,000 - 500,000) were added into the flask. After 5 min stirring, 20 µL of 0.5 M $HAuCl_4$ aqueous solution (prepared by $HAuCl_4 \bullet 3H_2O$ (Sigma-Aldrich)) was added and kept stirring for 15 min at room temperature. Then the solution was quickly loaded into a 195 ℃ oil bath for 30 min until the colour of the solution changed from light yellow to colourless, purple and finally brown. After the reaction, the solution was loaded into a water bath and cooled down to room temperature. After the solution was thoroughly cooled down, a further 5 µL of 0.5 M $HAuCl_4$ aqueous solution was added and the solution kept stirring for 20 hours. The final colloid was centrifuged at 9,000 rpm for 20 min and the precipitate was washed with ethanol and water three times with centrifugation at 3,000 rpm for 5 min. No further filtration was needed.

Gold nanorods (NR) were synthesized following the binary surfactant method.[42] To create gold seeds, in a scintillation vial were added 5 mL of 0.5 mM $HAuCl_4$ followed by 5 mL of 0.2 M CTAB (Sigma-Aldrich, ≥98%). Then, 0.3 mL of 20 mM freshly prepared $NaBH_4$ (Sigma-Aldrich, ≥98%) was added under stirring (1,200 rpm). The solution was aged at room temperature for 2 hours before use. For gold NR growth, 9 g CTAB and 1.543 g NaOL (sodium oleate, Sigma-Aldrich, ≥99%) were added into a 1 L flask with 250 mL water at 50 ℃ and mixed until dissolved. Then, the flask was set into a 30 ℃ water bath and 18 mL of 4 mM $AgNO_3$ (Sigma-Aldrich, ≥99%) were added. The solution was left undisturbed for 15 min at 30 ℃ after which 250 mL of 1 mM $HAuCl_4$ solution was added. The solution was kept stirring at 700 rpm for 90 mins until colourless. 2.5 mL HCl (32%) was added to adjust the pH. After 15 min of stirring at 400 rpm, 1.25 mL freshly prepared 0.1 M L-ascorbic acid (Sigma-Aldrich, reagent grade) were added to the solution, followed by vigorous stirring for 30 s. Finally, 0.4 mL gold seed solution were added, and the solution was then left undisturbed overnight at 30 ℃. To coat the gold NRs with p-DADMAC, the gold NR solution was washed in water (with centrifugation at 4000 rpm). A 1% p-DADMAC solution was added to the precipitate and sonicated for 10 mins. Finally, the solution was washed in

water (at 9000 rpm) another 3 times. The structural characterization of gold NSs and gold NRs is shown in Figure S1. Zeta potentials were determined using a Brookhaven Zeta PALS instrument.

Template Patterning

The templates were patterned *via* electron-beam lithography (EBL). To prepare the mother template, polished ITO-glass slides (Delta Technologies, CG-51IN-S115) were used as the substrate. The ITO slides were thoroughly cleaned by consecutive sonication in ethanol, isopropanol (IPA) and water. Then a 50 nm PMMA blocking polymer layer was prepared by spin coating PMMA (MicroChem) at 1,000 rpm onto the ITO and baked at 180 ℃ for 5 mins. A thin layer of chromium was then evaporated onto the ITO slide using a thermal evaporator (Intlvac Nanochrome II) and stored in a dust-free environment for further use. To pattern the ITO-PMMA template, the slides were exposed to an electron-beam (Vistec EBPG 5000plus ES) with a custom pattern created using modelling software (Klayout). After that, the chromium layer was removed in 5% H_2SO_4 followed by development with 3:1 methyl isobutyl ketone (MIBK) and IPA for 1min and then the slide was finally rinsed with IPA three more times. The array template was characterized by Atomic Force Microscopy as shown in Figure S2. The thickness of the PMMA layer was 50-60 nm.

EPD Cell assembly

The EPD process was carried in a 3D printed cell (UP-Plus). It was constructed from acrylonitrile butadiene styrene polymer (ABS). The printing layer thickness was 0.2 mm with a 45-degree printing angle. This cell was designed to fit into the dark-field microscope. There were two optical windows on the top and bottom panels, which enabled real-time observation of EPD under a dark-field microscope during the EPD process. A fixed chamber with a size of 8 mm (L) × 8 mm (W) × 2 mm (H) was created in the middle section of the cell. Two microflow channels were connected to the chamber for gold colloid injection. The assembly of the EPD cell is shown in Figure S3. The patterned template and counter electrode were connected by copper tape with two copper wires separately. To avoid fluid leakage, the cell was sealed by placing Teflon tape between the cell and slides. The cell was finally tightened with four screws at the corners.

For large area EPD assembly, most of the cell assembly processes were the same as those

used in the small-area EPD cell, except that multiple electrical contacts were required to minimize the IR drop across the ITO electrode. The EPD chamber was increased in size to 20 mm (L) × 20 mm (W) × 2 mm (H). 8 wires were hooked around both electrodes to generate an even electrode field across the template (Figure S4). For the EPD process, both electrodes were directly connected to a Keithley 2400 Source Meter. The patterned template was connected to the cathode and the counter electrode was connected to the anode. Approximately 0.3 mL gold colloid solution was injected into the flow-through channel. To initiate the EPD process, a constant potential was applied through the cell. Finally, to remove excess gold colloid, the template was rinsed by IPA and water, then dried by nitrogen blowing. This set-up enabled the EPD process to be monitored in real-time. A movie showing the EPD process is included as Supplementary Information.

Dark-field scattering spectroscopy

The scattering spectra of single gold nanocrystals were collected with a Nikon Lv100 Eclipse inverted microscope, equipped with a dark-field condenser and LU plus ELWD 50×/0.55 Nikon Lens in the reflection configuration. The light source of the microscope was a 100 W quartz halogen lamp. The scattered light was captured by an Acton Micro-Spec 2150i imaging spectrograph fitted with a PIXIS 1024F CCD. Another CCD Camera (ThorLabs) was attached to the microscope to capture the dark-field images. A polarizer was placed in the pathway of the reflected light for polarization-dependence measurements.

Electron microscopy and Atomic force microscopy

For transmission electron microscopy (TEM) images, 10 μL of gold nanoparticle solution were dried on carbon coated, 300 mesh copper grids (Electron Microscopy Sciences). Samples were imaged on a Tecnai F20 (FEI) at 200 kV accelerating voltage. Scanning electron microscopy (SEM) images were collected on a FEI Nova Nanolab (FEI) at 5 kV and 1.6 nA current. All atomic force microscopy (AFM) images were collected with an MFP-3D AFM (Asylum Research) loaded with silicon cantilevers (AC240TS-R3, Asylum Research).

ACKNOWLEDGEMENTS

The authors thank the ARC for support through grants LE110100161, LF100100117, CP110200319 and CE170100026. We thank the Melbourne Centre for Nanofabrication for access to EBL.

AUTHOR CONTRIBUTIONS

HZ designed the experiments and experimental devices, built the experiment set-up, performed the assembly experiments, and co-wrote the manuscript. CK synthesised gold nanoparticles, designed the surface chemistry and assisted with assembly experiments, and helped write manuscript. JC and TJ carried out nanofabrication of the ITO-PMMA template by EBL. AR oversaw the optics and helped write the manuscript. PM conceived the research, supervised the research work and co-wrote the manuscript.

ASSOCIATED CONTENT

The Supporting Information is available free of charge on the ACS Publications website at DOI:

This includes additional information on single nanoparticle electrophoretic deposition cell assembly, gold nanoparticle scattering spectrum, structure characterization of single nanoparticle arrays and a movie of the EPD deposition viewed in real time in a dark field microscope.

COMPETING FINANCIAL INTERESTS

The authors declare no competing financial interests.

REFERENCES

(1) Rivest, J. B.; Jain, P. K. Cation Exchange on the Nanoscale: An Emerging Technique for New Material Synthesis, Device Fabrication, and Chemical Sensing. *Chem. Soc. Rev.* **2013,** *42*, 89-96.

(2) Liu, J.; Lu, Y. A Colorimetric Lead Biosensor Using Dnazyme-Directed Assembly of Gold Nanoparticles. *J. Am. Chem. Soc.* **2003,** *125*, 6642-6643.

(3) Pingarrón, J. M.; Yañez-Sedeño, P.; González-Cortés, A. Gold Nanoparticle-Based Electrochemical Biosensors. *Electrochim. Acta* **2008,** *53*, 5848-5866.

(4) Siavoshi, S.; Yilmaz, C.; Somu, S.; Musacchio, T.; Upponi, J. R.; Torchilin, V. P.; Busnaina, A. Size-Selective Template-Assisted Electrophoretic Assembly of Nanoparticles for Biosensing Applications. *Langmuir* **2011,** *27*, 7301-7306.

(5) Collins, S. S.; Cittadini, M.; Pecharromán, C.; Martucci, A.; Mulvaney, P. Hydrogen Spillover between Single Gold Nanorods and Metal Oxide Supports: A Surface Plasmon Spectroscopy Study. *ACS Nano* **2015,** *9*, 7846-7856.

(6) Ma, W.; Kuang, H.; Wang, L.; Xu, L.; Chang, W.-S.; Zhang, H.; Sun, M.; Zhu, Y.; Zhao, Y.; Liu, L. Chiral Plasmonics of Self-Assembled Nanorod Dimers. *Sci. Rep.* **2013,** *3*, 1934.

(7) Zijlstra, P.; Chon, J. W.; Gu, M. Five-Dimensional Optical Recording Mediated by Surface Plasmons in Gold Nanorods. *Nature* **2009,** *459*, 410-413.

(8) Hoang, C. V.; Hayashi, K.; Ito, Y.; Gorai, N.; Allison, G.; Shi, X.; Sun, Q.; Cheng, Z.; Ueno, K.; Goda, K. Interplay of Hot Electrons from Localized and Propagating Plasmons. *Nat. Commun.* **2017,** *8*, 771.

(9) James, T. D.; Mulvaney, P.; Roberts, A. The Plasmonic Pixel: Large Area, Wide Gamut Color Reproduction Using Aluminum Nanostructures. *Nano Lett.* **2016,** 16, 3817-3823.

(10) Olson, J.; Manjavacas, A.; Basu, T.; Huang, D.; Schlather, A. E.; Zheng, B.; Halas, N. J.; Nordlander, P.; Link, S. High Chromaticity Aluminum Plasmonic Pixels for Active Liquid Crystal Displays. *ACS Nano* **2015,** *10*, 1108-1117.

(11) Liz-Marzán, L. M. Tailoring Surface Plasmons through the Morphology and Assembly of Metal Nanoparticles. *Langmuir* **2006,** *22*, 32-41.

(12) Dai, Z. R.; Pan, Z. W.; Wang, Z. L. Novel Nanostructures of Functional Oxides Synthesized by Thermal Evaporation. *Adv. Funct. Mater.* **2003,** *13*, 9-24.

(13) Brinker, C. J.; Lu, Y.; Sellinger, A.; Fan, H. Evaporation-Induced Self-Assembly: Nanostructures Made Easy. *Adv. Mater.* **1999,** *11*, 579-585.

(14) Li, M.; Bhiladvala, R. B.; Morrow, T. J.; Sioss, J. A.; Lew, K.-K.; Redwing, J. M.; Keating, C. D.; Mayer, T. S. Bottom-up Assembly of Large-Area Nanowire Resonator Arrays. *Nat. Nanotechnol.* **2008,** *3*, 88-92.

(15) Xiao, J.; Li, Z.; Ye, X.; Ma, Y.; Qi, L. Self-Assembly of Gold Nanorods into Vertically Aligned, Rectangular Microplates with a Supercrystalline Structure. *Nanoscale* **2014,** *6*, 996-1004.

(16) Kosiorek, A.; Kandulski, W.; Glaczynska, H.; Giersig, M. Fabrication of Nanoscale Rings, Dots, and Rods by Combining Shadow Nanosphere Lithography and Annealed Polystyrene Nanosphere Masks. *Small* **2005,** *1*, 439-444.

(17) Pardo, D. A.; Jabbour, G. E.; Peyghambarian, N. Application of Screen Printing in the Fabrication of Organic Light-Emitting Devices. *Adv. Mater.* **2000,** *12*, 1249-1252.

(18) Kuemin, C.; Stutz, R.; Spencer, N. D.; Wolf, H. Precise Placement of Gold Nanorods by Capillary Assembly. *Langmuir* **2011,** *27*, 6305-6310.

(19) Nepal, D.; Onses, M. S.; Park, K.; Jespersen, M.; Thode, C. J.; Nealey, P. F.; Vaia, R. A. Control over Position, Orientation, and Spacing of Arrays of Gold Nanorods Using

Chemically Nanopatterned Surfaces and Tailored Particle–Particle–Surface Interactions. *ACS Nano* **2012,** *6*, 5693-5701.

(20) Bavykin, D. V.; Passoni, L.; Walsh, F. C. Hierarchical Tube-in-Tube Structures Prepared by Electrophoretic Deposition of Nanostructured Titanates into a TiO_2 Nanotube Array. *Chem. Commun.* **2013,** *49*, 7007-7009.

(21) Urban, A. S.; Lutich, A. A.; Stefani, F. D.; Feldmann, J. Laser Printing Single Gold Nanoparticles. *Nano Lett.* **2010,** *10*, 4794-4798.

(22) Kuemin, C.; Nowack, L.; Bozano, L.; Spencer, N. D.; Wolf, H. Oriented Assembly of Gold Nanorods on the Single-Particle Level. *Adv. Funct. Mater.* **2012,** *22*, 702-708.

(23) Flauraud, V.; Mastrangeli, M.; Bernasconi, G. D.; Butet, J.; Alexander, D. T.; Shahrabi, E.; Martin, O. J.; Brugger, J. Nanoscale Topographical Control of Capillary Assembly of Nanoparticles. *Nat. Nanotechnol.* **2017,** *12*, 73-80.

(24) Sarkar, P.; Nicholson, P. S. Electrophoretic Deposition (EPD): Mechanisms, Kinetics, and Application to Ceramics. *J. Am. Ceram. Soc.* **1996,** *79*, 1987-2002.

(25) Song, K. W.; Costi, R.; Bulović, V. Electrophoretic Deposition of CdSe/Zns Quantum Dots for Light-Emitting Devices. *Adv. Mater.* **2013,** *25*, 1420-1423.

(26) Sarkar, P.; Haung, X.; Nicholson, P. S. Structural Ceramic Microlaminates by Electrophoretic Deposition. *J. Am. Ceram. Soc.* **1992,** *75*, 2907-2909.

(27) Giersig, M.; Mulvaney, P. Preparation of Ordered Colloid Monolayers by Electrophoretic Deposition. *Langmuir* **1993,** *9*, 3408-3413.

(28) Barbee, K. D.; Hsiao, A. P.; Heller, M. J.; Huang, X. Electric Field Directed Assembly of High-Density Microbead Arrays. *Lab on a Chip* **2009,** *9*, 3268-3274.

(29) Brown, P.; Kamat, P. V. Quantum Dot Solar Cells. Electrophoretic Deposition of CdSe− C_{60} Composite Films and Capture of Photogenerated Electrons with nC_{60} Cluster Shell. *J. Am. Chem. Soc.* **2008,** *130*, 8890-8891.

(30) Shah, A. A.; Ganesan, M.; Jocz, J.; Solomon, M. J. Direct Current Electric Field Assembly of Colloidal Crystals Displaying Reversible Structural Color. *ACS Nano* **2014,** *8*, 8095-8103.

(31) Shah, A. A.; Kang, H.; Kohlstedt, K. L.; Ahn, K. H.; Glotzer, S. C.; Monroe, C. W.; Solomon, M. J. Liquid Crystal Order in Colloidal Suspensions of Spheroidal Particles by Direct Current Electric Field Assembly. *Small* **2012,** *8*, 1551-1562.

(32) Prieve, D.; Anderson, J.; Ebel, J.; Lowell, M. Motion of a Particle Generated by Chemical Gradients. Part 2. Electrolytes. *J. Fluid Mech.* **1984,** *148*, 247-269.

(33) Prieve, D. C.; Sides, P. J.; Wirth, C. L. 2-D Assembly of Colloidal Particles on a Planar Electrode. *Curr. Opin. Colloid Interface Sci.* **2010,** *15*, 160-174.

(34) Qian, F.; Pascall, A. J.; Bora, M.; Han, T. Y.-J.; Guo, S.; Ly, S. S.; Worsley, M. A.; Kuntz, J. D.; Olson, T. Y. On-Demand and Location Selective Particle Assembly *Via* Electrophoretic Deposition for Fabricating Structures with Particle-to-Particle Precision. *Langmuir* **2015,** *31*, 3563-3568.

(35) Xiong, X.; Makaram, P.; Busnaina, A.; Bakhtari, K.; Somu, S.; McGruer, N.; Park, J. Large Scale Directed Assembly of Nanoparticles Using Nanotrench Templates. *Appl. Phys. Lett.* **2006,** *89*, 193108.

(36) Lee, Y. J.; Schade, N. B.; Sun, L.; Fan, J. A.; Bae, D. R.; Mariscal, M. M.; Lee, G.; Capasso, F.; Sacanna, S.; Manoharan, V. N. Ultrasmooth, Highly Spherical Monocrystalline Gold Particles for Precision Plasmonics. *ACS Nano* **2013,** *7*, 11064-11070.

(37) von Smoluchowski, M. Versuch Einer Mathematischen Theorie Der Koagulation Kinetic Kolloider Losungen. *Zeit. Phys. Chem.* **1917,** *92*, 129-168.

(38) O'Brien, R. W.; White, L. R. Electrophoretic Mobility of a Spherical Colloidal Particle. *J. Chem. Soc., Faraday Trans. 2* **1978,** *74*, 1607-1626.

(39) Besra, L.; Liu, M. A Review on Fundamentals and Applications of Electrophoretic

Deposition (EPD). *Prog. Mater. Sci.* **2007,** *52*, 1-61.

(40) Hunter, R. J. *Zeta Potential in Colloid Science: Principles and Applications*. Academic press: 2013; Vol. 2.

(41) Funston, A. M.; Novo, C.; Davis, T. J.; Mulvaney, P. Plasmon Coupling of Gold Nanorods at Short Distances and in Different Geometries. *Nano Lett.* **2009,** *9*, 1651-1658.

(42) Ye, X.; Zheng, C.; Chen, J.; Gao, Y.; Murray, C. B. Using Binary Surfactant Mixtures to Simultaneously Improve the Dimensional Tunability and Monodispersity in the Seeded Growth of Gold Nanorods. *Nano Lett.* **2013,** *13*, 765-771.

For Table of Contents Only

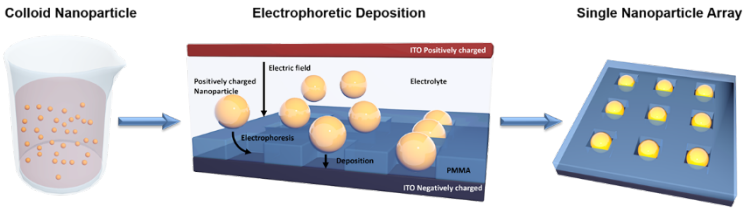

1.